*Journal of Biomolecular NMR*, **26:** 49–68, 2003.
*KLUWER/ESCOM*



# Analysis of local conformation of membrane-bound and polycrystalline peptides by two-dimensional slow-spinning rotor-synchronized MAS exchange spectroscopy

Charles M. Gabrys, Jun Yang and David P. Weliky*
*Department of Chemistry, Michigan State University, East Lansing, MI 48824, U.S.A.*

Received 3 January 2003; Accepted 30 January 2003

*Key words:* conformation, exchange, fusion, MAS, melittin, membrane, NMR, peptide, solid-state, two-dimensional

## Abstract

2D slow-spinning, rotor-synchronized MAS exchange spectroscopy (SSRS-MASE) was applied to study local secondary structure of three structurally different peptides, two of which were membrane-bound. Each peptide was $^{13}C$ carbonyl labeled at two adjacent residues in the peptide backbone. In general, this methodology is attractive for membrane-bound peptides because of its lenient spinning, decoupling, and RF homogeneity requirements.

For a single set of raw SSRS-MASE data, two linearly independent methods exist for obtaining a 2D spectrum and each spectrum can be fit to obtain conformational constraints. An approach is described for combining the results of these two fits and this method is shown to work for spectra with both resolved and unresolved labeled site resonances. A spectrum is often fit well to a few different conformations which have somewhat different values of the fitting parameter $\chi^2$. A simple statistical theory is developed which relates the $\Delta\chi^2$ difference between a local minimum and the global minimum $\chi^2$ to the likelihood that the local minimum conformation is the correct structure. Because uncertainty in the simulated data can also contribute to the overall fitting uncertainty, an empirical method is described for incorporating the simulation uncertainty into the $\Delta\chi^2$ analysis.

These data analysis methods were tested on polycrystalline Ala-Gly-Gly and then applied to the membrane-bound melittin and HIV-1 fusion peptides. Melittin gave a best-fit α helical structure at Ala-4 while the fusion peptide gave a good-fit β strand structure at Phe-8. The melittin analysis is in agreement with the known overall structure of this peptide.

*Abbreviations:* AGG – alanylglycylglycine; BCA – bicinchoninic acid; CP – cross-polarization; CSA – chemical shift anisotropy; DQ – double quantum; DRAWS – dipolar recoupling with a windowless multipulse irradiation; DTPC – di-o-tetradecyl-sn-glycero-3-phosphocholine; FMOC – 9-fluorenylmethoxycarbonyl; FP – fusion peptide; HIV – human immunodeficiency virus, HPLC – high-performance liquid chromatography; MAS – magic angle spinning; RFDR – radiofrequency-driven dipolar recoupling; RMSD – root-mean-squared deviation; SSRS-MASE – slow-spinning, rotor-synchronized magic angle spinning exchange; 1D – one-dimensional; 2D – two-dimensional.

## Introduction

Magic angle spinning (MAS) solid state nuclear magnetic resonance (NMR) spectroscopy has become a useful probe of local conformation in membrane-bound peptide and protein systems. Recent studies include rhodopsin-bound retinal, the serine bacterial chemoreceptor, magainin, and the HIV-1 fusion peptide (Hirsh et al., 1996; Creemers et al., 1999; Eilers et al., 1999; Murphy et al., 2001; Yang et al., 2001a, b). Chemical shifts are the most basic structural probe

*To whom correspondence should be addressed. E-mail: weliky@cem.msu.edu

and provide evidence of helical or non-helical structure (Spera and Bax, 1991; Wishart et al., 1991). More sophisticated techniques rely on measurement of conformation-dependent dipolar couplings (Griffin, 1998) or on conformation-dependent relative orientation of shift tensors (Tomita et al., 1994; Tycko et al., 1996; Gregory et al., 1997; Bower et al., 1999; Blanco and Tycko, 2001). In this paper, we discuss one of the latter methods, the application of two-dimensional slow spinning, rotor-synchronized magic angle spinning exchange (2D SSRS-MASE) spectroscopy to analysis of local conformation in membrane-bound and polycrystalline peptides. The methodology was originally conceived as a probe of slow motion (Kentgens et al., 1987; Hagemeyer et al., 1989; Luz et al., 1992) and was then applied to determine local conformation in polycrystalline, lyophilized, and frozen solution peptide and protein systems (Weliky and Tycko, 1996; Long and Tycko, 1998; Weliky et al., 1999; Balbach et al., 2000).

For unoriented samples, exchange under both static and spinning conditions relies on specific labeling of two nearby homonuclei ($^{13}$C in our case) and a simple 2D experiment in which the magnetization evolves under the anisotropic chemical shift of one of the labeled sites during $t_1$, diffuses to the second site during the exchange period $\tau$, and evolves under the anisotropic chemical shift of the second site during $t_2$. If all of the molecules in the sample have the same local structure near the two labeled sites, then the chemical shift anisotropy (CSA) tensors of the two sites will have a well-defined relative orientation which will be manifested as correlation between the anisotropic chemical shifts of the two nuclei. This correlation will produce an off-diagonal intensity pattern in the 2D exchange spectrum which is distinctively characteristic of the relative CSA tensor orientation and the particular local structure. Because of the low probability of nearby natural abundance $^{13}$C/$^{13}$C spin pairs, the off-diagonal intensity will be dominated by these labeled-site signals. In order to relate the off-diagonal pattern to local structure, simulated 2D spectra must be generated as a function of local structure and comparison made between the simulated and experimental spectra. The simulations require knowledge of the CSA principal values of each of the labeled sites as well as the orientation of the CSA principal axis system of each labeled site relative to its chemical bonds. In many cases, the principal values can be directly measured from 1D spectra and the principal axis system orientations are approximately known from studies of model compounds.

Structural applications of this type of 2D exchange spectroscopy were originally made using static samples, and an off-magic angle spinning variant of the technique has also been reported (Edzes and Bernards, 1984; Henrichs and Linder, 1984; Tycko and Dabbagh, 1991; Asakura et al., 2001). For the static case, the off-diagonal intensity pattern can be straightforwardly simulated using the anisotropic chemical shift formula and powder averaging.

Under MAS, there is periodic modulation of the anisotropic shift interactions which concentrates the NMR signal at the isotropic and spinning sideband frequencies of the two labeled sites. These $\nu_M^n$ frequencies for site $n = 1$ or 2 can be calculated as $\nu_M^n = \nu_{iso}^n + M\nu_r$, where $\nu_{iso}^n$ and $\nu_r$ are the isotropic and MAS frequencies, and $M = 0, \pm1, \pm2, \ldots$ If the shift tensors of the two sites are not colinear, then the 2D exchange spectrum will contain off-diagonal crosspeaks which have frequency $\nu_M^n$ in one dimension and frequency $\nu_{M'}^{n'}$ ($M' \neq M'$, $n \neq n'$) in the second dimension. If the CSA principal values and principal axis orientations of each labeled site are known, then the relative off-diagonal crosspeak intensities can be simulated as a function of local structure. The equations for the MAS crosspeak intensities are well-understood and have been published in detail elsewhere (Hagemeyer et al., 1989; Luz et al., 1992; Tycko et al., 1996; Tycko and Berger, 1999). It is noted that a simple formula does not exist to relate the MAS off-diagonal crosspeak intensities to the off-diagonal intensity pattern of a static spectrum.

This paper applies 2D MAS exchange spectroscopy (specifically 2D SSRS-MASE) to determine local secondary structure in membrane-bound and polycrystalline peptides. Relative to static exchange, the slow-spinning MAS version has several advantages including, most importantly, increased sensitivity due to sharp MAS lines. In membrane-bound peptide studies, one typically wishes to work with fully hydrated lipids and with peptide:lipid mol ratios $\leq 1:20$. In our experience, this constrains the peptide quantity to $\leq 2$ μmol in a 200 μl volume. Sensitivity is paramount for these sample quantities, which are significantly less than the 5–20 μmol quantities accessible in studies of pure solid peptides. In addition, the 2D exchange experiment uses only a few pulses, can be done with 60 kHz $^1$H decoupling, is insensitive to RF inhomogeneity, and uses spinning speeds of $\leq 5$ kHz. Because of these lenient conditions, com-

mercial probes with large-volume (> 200 μl) rotors can be used to provide either greater sample quantity and NMR signal, or lower peptide:lipid ratio, which may have greater biological relevance. 2D SSRS-MASE does require rotor synchronization of pulses over ∼ 1 s to suppress artifactual crosspeak intensity.

The samples contain $^{13}C$ carbonyl labeling at two adjacent residues in the peptide backbone. For 2D SSRS-MASE, there are several advantages of $^{13}C$ carbonyl over $^{15}N$ amide or $^{13}C_\alpha$ labeling including: (1) The detection sensitivity for $^{13}C$ is higher than for $^{15}N$; (2) the carbonyl CSA tensor is large and the orientation of its principal axis system relative to its chemical bonds is well-characterized and approximately independent of peptide structure (Oas et al., 1987); and (3) $^{13}C$ carboxyl labeled amino acids are more widely available and less expensive than $^{13}C_\alpha$ labeled amino acids.

For carbonyls at adjacent peptide residues, the local secondary structure dihedral angles ($\varphi$, $\psi$) are the main unknown parameters which determine the relative orientation of the carbonyl CSA tensors and hence the off-diagonal crosspeak intensities in a 2D SSRS-MASE spectrum. Using the known bond geometry in peptides and the known orientation of the carbonyl CSA tensor relative to its local bonding, formulas have been derived for the 2D SSRS-MASE crosspeak intensities as a function of ($\varphi$, $\psi$) (Tycko et al., 1996; Tycko and Berger, 1999). With the additional input of experimental CSA principal values, the simulated crosspeak intensities can be calculated and compared to the experimental intensities. Reasonable agreement between experiment and simulation typically only occurs in a few restricted regions of ($\varphi$, $\psi$) conformational space.

In the 2D SSRS-MASE analysis, the ($\varphi$, $\psi$) are treated as unknown parameters and are fitted, while the CSA and bond geometry are treated as known parameters. There are small uncertainties in these latter parameters which can be considered as simulation uncertainty in the fitting. This aspect of the analysis is discussed in the Theory and Results sections of this paper.

In 2D SSRS-MASE, four free-induction decays (FIDs) are taken for each $t_1$ time, and these data can be processed in two different ways to produce two linearly-independent, 2D exchange spectra (Tycko and Berger, 1999). In the Hagemeyer, Schmidt-Rohr, and Spiess (HSS) method, the experimental crosspeak intensity is largely due to magnetization exchange between the two labeled sites (Hagemeyer et al., 1989). This is advantageous because the variation of this intersite intensity with spinning sideband number provides the basis of the conformational analysis. There is also intersite crosspeak intensity with the Herzfeld, Roberts, and Griffin (HRG) processing method (Herzfeld et al., 1987), and HRG intensity variation with conformation is different from that of the HSS method. Thus, use of HSS and HRG 'dual processing' should provide independent verification of the correct secondary structure.

One complication of the HRG method is that large crosspeak intensity is also present for magnetization which remains on the same carbonyl nucleus in the $t_1$ and $t_2$ dimensions. For both the HSS and HRG methods, the crosspeaks directly adjacent to the spectrum diagonal have a small intensity contribution because of rapid longitudinal $^{14}N$ relaxation during $\tau$. This contribution arises from magnetization which is on the same carbonyl nucleus during $t_1$ and $t_2$ but which experiences a different $^{13}C$-$^{14}N$ dipolar coupling and hence local field tensor during the different times. In the context of 2D SSRS-MASE, the intrasite intensity does not provide any useful structural information.

For the case of resolved chemical shifts of the two labeled sites, the uninteresting intrasite crosspeaks do not interfere with the structural analysis because they are separated from the interesting intersite crosspeaks. In the case of unresolved chemical shifts, the intrasite crosspeaks overlap with the intersite crosspeaks, and the intrasite contribution must be subtracted in the structural analysis.

This paper demonstrates the accuracy and limitations of 2D SSRS-MASE secondary structure analysis of three different peptides, two of which were associated with membranes. In spectra of one membrane-bound peptide, melittin, the shifts of the two labeled carbonyls were resolved while in the other case, the HIV-1 fusion peptide (FP23), the shifts were not resolved. In addition, we recorded spectra of the model polycrystalline tripeptide Ala-Gly-Gly (AGG) and fitted both the naturally resolved spectra and spectra which had been broadened such that the intrasite and intersite crosspeaks were not resolved.

For resolved shifts, the accuracy of the 2D SSRS-MASE methodology in determining the conformation of small model systems was demonstrated in earlier studies on AGG (Weliky and Tycko, 1996; Tycko and Berger, 1999). An attempt was also made to simulate the HSS processing for unresolved shifts (Weliky and Tycko, 1996). The experimental and calculated intersite crosspeak intensities from a resolved spectrum were summed to produce a quasi-unresolved

spectrum, and fitting was done using the summed crosspeaks. This was not a realistic simulation of the unresolved case for two reasons. First, the simulation neglected intrasite crosspeak intensity arising from relaxation of directly-bonded $^{14}$N. Second, the simulation used CSA principal values derived from resolved 1D MAS spectra. However, for the real case of unresolved sites, only one set of principal values can be obtained from the unresolved 1D MAS spectra. The present study provides a more realistic simulation of the case of unresolved sites for both HSS- and HRG-processed data.

Both melittin and FP23 have interesting and biologically relevant interactions with membranes. Melittin (GIGAVLKVLTTGLPALISWIKRKRQQ) is the major component of bee venom and is well-known for its hemolytic activity (Dempsey, 1990). It has also been shown at high concentrations ($\geq$ 3 mol%) to induce micellization of membrane bilayers (Dempsey, 1990; Yang et al., 2001b). Studies of melittin by a variety of techniques, including solid state NMR, are consistent with a predominantly helical conformation of the membrane-bound form of the peptide (Dempsey, 1990; Smith et al., 1994; Bechinger, 1997).

FP23 (AVGIGALFLGFLGAAGSTMGARS) is the N-terminal 'fusion peptide' domain of the $LAV_{1a}$ strain of the HIV-1 gp41 envelope protein. Mutagenesis studies on the fusion peptide domain of the HIV-1 virus have demonstrated that this domain plays a critical role in inducing viral/target cell fusion (Freed et al., 1990, 1992; Schaal et al., 1995). In addition, the FP23 peptide by itself induces fusion between unilamellar liposomes or between erythrocytes (Rafalski et al., 1990; Mobley et al., 1995). Strong correlation between the mutagenesis/fusion activity relationships of the viral fusion peptide domain and the FP23 peptide provides evidence that the FP23 peptide is a useful model system for understanding some aspects of membrane fusion (Durell et al., 1997). FP23 appears to have significant structural plasticity in membranes and can adopt both helical and non-helical structures (Rafalski et al., 1990; Nieva et al., 1994; Durell et al., 1997). It is not clear whether one or both of these structural types are fusogenic. At the 1 : 20 peptide:lipid mol ratio of the present study, the preponderance of experimental data is consistent with non-helical structure (Martin et al., 1996; Durell et al., 1997; Yang et al., 2001a).

## Theory

A key feature in the analysis of 2D SSRS-MASE data and in the analysis of nonlinear least squares fits in general is the possibility that several distinct sets of parameters (the ($\varphi$, $\psi$) in this study) will each fit the data reasonably well. Each of these good-fit ($\varphi$, $\psi$) conformations is associated with either the global minimum or a local minimum in the fitting parameter $\chi^2$:

$$\chi^2(\varphi, \psi) = \chi^2 = \sum\nolimits_j \left[ y_j^{\text{expt.}} - y_j^{\text{calc.}}(\varphi, \psi) \right]^2 / \sigma^2, \quad (1)$$

where $y_j^{\text{expt.}}$ are the experimental data points (intersite crosspeak intensities), $y_j^{\text{calc.}}$ ($\varphi$, $\psi$) are the simulated data points for ($\varphi$, $\psi$), and $\sigma^2$ is the mean-squared uncertainty, which is assumed to be the same for each point, and which could contain contributions from experiment and from simulation. The existence of several distinct $\chi^2$ minima in the analysis was previously investigated for polycrystalline AGG (Tycko et al., 1996) and may be expected whenever the fitting function is not linear in the fitted parameters. Minima were observed near the correct ($\varphi$, $\psi$) as well as at other distinct ($\varphi$, $\psi$) whose relative orientation of labeled carbonyl CSA tensors happened to be close to that found in the true structure. In the terminology of nonlinear least squares, the fit is ill-conditioned, and other information is required to determine $\varphi$ and $\psi$ with absolute certainty. Even after consideration of intercarbonyl dipolar couplings, it is still possible that at least two distinct structures represent reasonable fits to the experimental data (Weliky et al., 1999).

With a single set of 2D SSRS-MASE experimental data, it is most reasonable to postulate that the conformation corresponding to the global minimum $\chi^2$ has the highest probability of being the correct structure. In this section, we derive a measure of the likelihood that a different local $\chi^2$ minimum conformation could instead be the correct structure. To our knowledge, this issue is not addressed in standard texts on the statistical treatment of scientific data and is different from the well-studied analysis of uncertainties in parameter values at one $\chi^2$ minimum (Bevington and Robinson, 1992; Press et al., 1996). For this latter analysis of 2D SSRS-MASE data, one would first assume that a particular $\chi^2$ minimum conformation is the correct structure. Each unit increase in $\chi^2$ about the minimum is then associated with unit increases in the number of root-mean-squared deviations (RMSDs) of the $\varphi$ and $\psi$ parameters ($1\sigma$, $2\sigma$, etc.).

For membrane-bound peptides, which are experimental targets of significant biological interest, the signal-to-noise of the 2D SSRS-MASE spectra is low enough that $\sigma^2$ is dominated by experimental noise. Therefore, in the next few paragraphs, we derive a simple expression for the effect that experimental uncertainty could have on the $\Delta_e\chi^2$ difference between the $\chi^2$ value at a local ($\varphi$, $\psi$) fitting minimum and the $\chi^2$ value at the global minimum. This expression is then related to the likelihood that the local minimum conformation is the correct structure.

We focus on two $\chi^2$ minimum conformations, denoted A and B, each of which corresponds to a particular ($\varphi$, $\psi$) and can be considered as a potential structure for the peptide. Suppose that one experimental data set is taken. If one assumes that a particular structure is correct (either A or B), statistical factors such as $(\chi^2)^A$ (for model A) or $(\chi^2)^B$ (for model B) provide information about the probability of obtaining this data set (Bevington and Robinson, 1992; Press et al., 1996). We define the parameter

$$\Delta\chi^2 = (\chi^2)^B - (\chi^2)^A \tag{2}$$

and suppose that $\Delta\chi^2 > 0$ for this data set. Because $\Delta\chi^2 > 0$, there is a higher probability for obtaining this data set with model A than with model B. On this basis, we infer that model A is more likely the correct structure. Suppose that the experiment is repeated and fits of the new data set yield $(\chi^2)^A$ and $(\chi^2)^B$ with $\Delta\chi^2 < 0$. Considering only this second data set, model B is more likely the correct structure. Under ideal circumstances, the experiment would be repeated many times so that the frequency with which conformation A or B is the global $\chi^2$ minimum would indicate the likelihood that it is the correct structure.

In practice, adequate 2D SSRS-MASE signal-to-noise on membrane-bound peptides often requires days of data collection. Therefore, a single data set is taken, and one set of experimental values $(\chi^2)^A$, $(\chi^2)^B$, and $\Delta_e\chi^2$ ($= (\chi^2)^B - (\chi^2)^A$) is calculated. For concreteness in the discussion, we assign superscript A to the conformation with the global minimum $\chi^2$ so that $\Delta_e\chi^2 > 0$. The next step is to make an approximate calculation of $\sigma_{\Delta\chi^2}$, the expected RMSD of $\Delta\chi^2$ when all possible data sets are considered. The ratio $\Delta_e\chi^2/\sigma_{\Delta\chi^2}$ is then related to the relative likelihoods that model A or model B is the correct structure.

To begin, consider that the experimental data consist of N crosspeak intensities whose values can be simulated correctly for any structural model, i.e., set of ($\varphi$, $\psi$) values. The experimental data are $E_1$, $E_2$, ..., $E_N$, the simulated data from model A are $V_1^A$, $V_2^A$, ..., $V_N^A$, and the simulated data from model B are $V_1^B$, $V_2^B$, ..., $V_N^B$. The parameter $\alpha_j$ is defined:

$$\alpha_j = V_j^B - V_j^A \tag{3}$$

and is the same for all experimental data sets. The RMSD uncertainty for each experimental data point has a value 's' for our data set. $(\chi^2)^A$ and $(\chi^2)^B$ are given by:

$$(\chi^2)^A = \sum_j (V_j^A - E_j)^2/s^2 \tag{4a}$$

$$\begin{aligned}(\chi^2)^B &= \textstyle\sum_j (V_j^B - E_j)^2/s^2 \\ &= \textstyle\sum_j (V_j^A + \alpha_j - E_j)^2/s^2 \\ &= \textstyle\sum_j (V_j^A - E_j)^2/s^2 + \sum_j \alpha_j^2/s^2 \\ &\quad + 2\textstyle\sum_j \left\{\alpha_j \times (V_j^A - E_j)/s^2\right\} \\ &= (\chi^2)^A + \alpha^2 \\ &\quad + (2/s^2)\textstyle\sum_j \left\{\alpha_j \times (V_j^A - E_j)\right\},\end{aligned} \tag{4b}$$

where

$$\alpha^2 = \sum_j \alpha_j^2/s^2. \tag{5}$$

Thus,

$$\begin{aligned}\Delta\chi^2 &= (\chi^2)^B - (\chi^2)^A \\ &= \alpha^2 + (2/s^2)\textstyle\sum_j \left\{\alpha_j \times (V_j^A - E_j)\right\}.\end{aligned} \tag{6}$$

Because of the variation of $E_j$ between different data sets, there is a distribution of possible $\Delta\chi^2$ values. Simulations were used to understand this distribution. Starting from a single structure (model A), a group of simulated 2D SSRS-MASE data sets was created in which the data points (i.e., crosspeak intensities) also had a contribution from random Gaussian noise. For each data set, $\Delta\chi^2$ was calculated between model A and another $\chi^2$ minimum structure (model B). Analysis of the distribution of $\Delta\chi^2$ values for 100 such sets showed an approximate Gaussian shape with average value $\langle\Delta\chi^2\rangle \approx \alpha^2$ and RMSD $\sigma_{\Delta\chi^2} \approx 2\alpha$. As the analytical derivation continues, these simulation results are shown to be the average and RMSD values of $\chi^2$ in Equation 6.

In the right-hand-most expression of Equation 6, the only terms which vary between different experimental data sets are $(V_j^A - E_j)$. We again consider that model A is the correct structure, and because the

noise in the experimental data points $E_j$ is considered to be random with no component of systematic error, an average over all possible data sets yields $\langle (V_j^A - E_j) \rangle = 0$. The average of $\Delta\chi^2$ over all data sets simplifies to:

$$\begin{aligned}\langle \Delta\chi^2 \rangle &= \langle \alpha^2 \rangle + \left\langle (2/s^2) \sum_j \left\{ \alpha_j \times (V_j^A - E_j) \right\} \right\rangle \\ &= \alpha^2 + (2/s^2) \sum_j \left\{ \alpha_j \times \left\langle (V_j^A - E_j) \right\rangle \right\} \\ &= \alpha^2. \end{aligned} \quad (7)$$

The relationships $\langle (V_j^A - E_j)^2 \rangle = s^2$ and $\langle (V_j^A - E_j)(V_k^A - E_k) \rangle = 0$ (for $j \neq k$) as well as Eqs. (5), (6), and (7) are used to obtain $\sigma_{\Delta\chi^2}$.

$$\begin{aligned}\sigma_{\Delta\chi^2} &= \sqrt{\left\langle (\Delta\chi^2 - \langle \Delta\chi^2 \rangle)^2 \right\rangle} \\ &= \sqrt{\left\langle (4/s^4) \left( \sum_j \left\{ \alpha_j \times (V_j^A - E_j) \right\} \right)^2 \right\rangle} \\ &= (2/s^2) \sqrt{\sum_j (\alpha_j^2 \times \left\langle (V_j^A - E_j)^2 \right\rangle) + \sum_j \sum_{k \neq j} \left\{ \alpha_j \alpha_k \times \left\langle (V_j^A - E_j)(V_k^A - E_k) \right\rangle \right\}} \\ &= 2\alpha \,. \end{aligned} \quad (8)$$

The average value of $\Delta\chi^2$ is $\alpha^2$, and for our experimental data set, the value of $\Delta\chi^2$ is $\Delta_e\chi^2$. In order to easily obtain a semi-quantitative value of $\Delta_e\chi^2/\sigma_{\Delta\chi^2}$, we approximate that $\Delta_e\chi^2 \approx \alpha^2$. It then follows from Equation 8:

$$\Delta_e\chi^2/\sigma_{\Delta\chi^2} = \alpha^2/(2\alpha) = \alpha/2 \approx \sqrt{\Delta_e\chi^2}/2. \quad (9)$$

The distribution of $\chi^2$ values obtained using data sets which include Gaussian noise is the well-studied '$\chi^2$ distribution' (Arley and Buch, 1966), but for ease of approximation, a Gaussian distribution can be found that matches a given $\chi^2$ distribution reasonably well. Thus, a table of integrals of a Gaussian distribution with mean and standard deviation linked as in Equations 7 and 8 is used to provide some numerical examples of Equation (9) (Bevington and Robinson, 1992). For example, if $\Delta_e\chi^2 = 4$, Equation 9 shows that $\Delta_e\chi^2/\sigma_{\Delta\chi^2} \approx 1$, which implies a 16% probability that a different experimental data set would yield $\Delta_e\chi^2 < 0$. This calculation gives some measure of the likelihood that model B rather than model A is the correct structure. If $\Delta_e\chi^2 = 16$, $\Delta_e\chi^2/\sigma_{\Delta\chi^2} \approx 2$, and there is a 2% probability that a different data set would yield $\Delta_e\chi^2 < 0$. As our measured $\Delta_e\chi^2$ increases, there is increasing confidence in the sign of $\Delta_e\chi^2$ and a greater probability that the model with the lower $\chi^2$ is the correct structure.

In the Results section, we incorporate these ideas into the presentation of $\chi^2$ ($\varphi$, $\psi$) contour plots. The darkest shade is used for values of $\chi^2$ within four units of the global minimum $\chi^2$ with the implication that the correct structure is most likely found within this area. The choice of four units is based on Equation 9; i.e., if $\Delta_e\chi^2 = 4$, $\Delta_e\chi^2/\sigma_{\Delta\chi^2} \approx 1$. Additional contours are also shown for $\chi^2$ values between four and eight units of the global minimum $\chi^2$ and for $\chi^2$ values between eight and twelve units of the global minimum. Minima found within these regions are less likely to correspond to the correct structure.

The derivation in this section considers the impact that different experimental data sets could have on $\chi^2$ ($\varphi$, $\psi$) and $\Delta\chi^2$ values. This is a reasonable approach for membrane-bound peptides for which uncertainty in the 2D SSRS-MASE analysis appears to be dominated by experimental noise. However, for pure solid peptides, there is often sufficient sample to obtain experimental data with high signal-to-noise and relatively small uncertainty in the $y_j^{expt.}$. In this case, there can be a significant contribution to the total fitting uncertainty from simulation uncertainty in the $y_j^{calc.}$ ($\varphi$, $\psi$). To model simulation uncertainty, we can consider that there are groups of simulated data sets $\{W^A\}$ and $\{W^B\}$ which are based on narrow distributions of simulation input parameters (e.g., CSA principal values). These distributions are centered around the true parameter values found in $V^A$ and $V^B$. Fits using $\{W^A\}$ and $\{W^B\}$ will produce a distribution of $\Delta\chi^2$ values whose mean and width can be approximately calculated in a manner similar to the previous derivation. For example, when simulation is the major source of uncertainty and when variation of simulation input parameters produces correlated changes in the $\chi^2$ values at the two minima, Equations 7 and 8 will still be approximately correct, with the 's' dominated by simulation instead of experimental uncertainty. This type of correlation between $\chi^2$ minima values is sometimes evident in our fitting.

## Materials and methods

### *Materials*

Rink amide resin was purchased from Advanced Chemtech (Louisville, KY), and 9-fluorenylmethoxy carbonyl (FMOC)-amino acids were obtained from Peptides International (Louisville, KY). $^{13}C$ carbonyl labeled amino acids were purchased from Icon Services Inc. (Summit, NJ) and the FMOC group was

added using literature methods (Chang et al., 1980; Lapatsanis et al., 1983). Di-o-tetradecyl-sn-glycero-3-phosphocholine (DTPC) was purchased from Avanti Polar Lipids, Inc. (Alabaster, AL). The Micro BCA protein assay was obtained from Pierce (Rockford, IL) and is a colorimetric approach for determining peptide concentration. Unlabeled AGG was obtained from Sigma (St. Louis, MO). All other reagents were analytical grade.

*Sample preparation*

Melittin was synthesized as its C-terminal amide using a peptide synthesizer (ABI 431A, Foster City, CA) equipped for FMOC chemistry. FP23 peptides corresponding to the 23 N-terminal residues of the $LAV_{1a}$ strain of the HIV-1 gp41 protein were synthesized by similar methods. AGG was synthesized as an acid and was subsequently recrystallized from water. All amino acids were single-coupled using two hour coupling times. Reversed-phase HPLC was used to purify melittin and FP23 while precipitation from acetone was used to purify AGG. Mass spectroscopy was used to verify peptide purity. Purified yields were $\sim$ 25%.

Melittin was $^{13}C$ labeled at the carbonyl carbons of Gly-3 and Ala-4. FP23 was $^{13}C$ labeled at the carbonyl carbons of Leu-7 and Phe-8. AGG was $^{13}C$ labeled at the carbonyl carbons of Ala-1 and Gly-2.

Melittin:DTPC and FP23:DTPC NMR samples were prepared using 0.01% $NaN_3$ in water at pH $\sim$ 6. DTPC is a convenient lipid for peptide carbonyl NMR because it is ether- rather than ester-linked and hence has no natural abundance carbonyl background. Mixtures of dissolved peptide and DTPC dispersion were mixed to form $\sim$ 200 $\mu$l total volume. The final peptide and DTPC concentrations were 10 mM and 200 mM, respectively. Phosphate buffer (50 mM, pH 7.0) was added to the FP23:DTPC sample after initial peptide/lipid binding. There was little change in the peptide carbonyl NMR spectrum and presumably the FP23 Leu-7, Phe-8 local structure after addition of the phosphate buffer.

For the melittin sample, peptide binding to membrane was immediately apparent in the change in the sample transparency from opaque to translucent. This change has been correlated in lipid NMR experiments with formation of non-lamellar structures (Dempsey, 1990; Yang et al., 2001b). For the FP23 sample, peptide binding was measured by adding $\sim$ 800 $\mu$l water to the peptide/lipid dispersion, vortexing the mixture, and then centrifuging at 12,000 $\times$ $g$. The BCA assay was used to determine the concentration and quantity of peptide in the supernatant and this was compared to the total quantity of peptide in the sample. Comparison of the two quantities demonstrated that $>$ 80% of the peptide was bound to the DTPC. Under these centrifugation conditions all of the lipid was pelleted, and there was no interference from unpelleted lipid in the BCA assay. Calibration of the BCA assay was done using a solution containing a known mass of FP23.

A qualitative assay was used to demonstrate the fusogenicity of FP23 at concentrations comparable to those used for NMR experiments. A clear sonicated 100 mM vesicle solution was prepared, and this solution immediately changed from clear to opaque upon addition of 0.3 mM FP23. This change is associated with formation of larger fused lipid structures. No change was observed in vesicle solution clarity upon addition of a mutant peptide with a Val-2 $\rightarrow$ Glu-2 point mutation. This data is consistent with previous studies which demonstrated that the mutation abolishes the fusogenicity of both the free peptide and the virus (Freed et al., 1992; Pereira et al., 1995).

The AGG sample was made by grinding a single AGG crystal which had been grown by slow evaporation of an aqueous solution containing labeled and unlabeled AGG in a 1:19 mol ratio. The NMR sample contained 17 $\mu$mol labeled AGG.

*NMR experiments and data analysis*

Measurements were made on a 9.4 T spectrometer (Varian VXR, Palo Alto, CA) using a double resonance magic angle spinning (MAS) probe equipped for 7 mm diameter $Si_3N_4$ rotors. The sample volume was 220 $\mu$l. The NMR detection channel was tuned to $^{13}C$ at 100.6 MHz, and the decoupling channel was tuned to $^{1}H$ at 400.0 MHz. Chemical shifts were externally referenced to the methylene carbon resonance of adamantane (38.2 ppm). For the melittin and FP23 samples, strong $^{13}C$ signals could not be observed above $-20$ °C, presumably because of signal attenuation due to slow motion. Hence, samples were cooled to $-50$ °C either slowly in the NMR probe or by fast freezing in liquid nitrogen. Both freezing techniques gave comparable spectra. The AGG spectra were taken at ambient temperature.

1D spectra were obtained using 1 ms of cross-polarization (CP) at 47 kHz followed by signal detection with decoupling at 65 kHz. The recycle delay was 0.5 s for the melittin and FP23 samples and 1 s for the AGG sample. For both the melittin and FP23 samples, the one-dimensional (1D) carbonyl signal contains $\sim$ 10% contribution from peptide natural

abundance sites. The natural abundance signal is not resolved from signals from the labeled sites.

2D exchange spectra were obtained at 2.5 kHz spinning frequency using the 2D SSRS-MASE pulse sequence (CP) – $t_1$ – ($\pi$/2) - $\tau$ - ($\pi$/2) – $t_2$, in which (CP) represents cross-polarization from $^1$H to $^{13}$C, $t_1$ is the evolution period, $\pi$/2 represents a $^{13}$C pulse, $\tau$ (500 ms) is the spin diffusion period, and $t_2$ is the $^{13}$C detection period (Tycko et al., 1996; Weliky and Tycko, 1996). The spinning speed was controlled to $\pm$1 Hz and the pulse program was actively synchronized to the tachometer signal. For the melittin and FP23 samples, the experiments were run under the following conditions: (1) 800 $\mu$s CP was made with $^{13}$C RF radiation at 50 kHz and a linear ramp on $^1$H between 45 kHz and 55 kHz (Metz et al., 1994); (2) 50 kHz $^{13}$C $\pi$/2 pulses were applied; (3) 72 $t_1$ points were taken with an increment of 40 $\mu$s; (4) signals were acquired for 10 ms during $t_2$; (5) decoupling at 70–75 kHz was applied during $t_1$ and $t_2$ but not during $\tau$; (6) the recycle delay was 0.5 s; and (7) phase cycling consisted of x, $-$x alternation of the first $^{13}$C $\pi$/2 pulse and CYCLOPS alternation of the final $^{13}$C $\pi$/2 and receiver phase (Hoult, 1975). Complete data sets were collected in twelve-hour blocks and then summed together, with 10–15 blocks in a final data set. Similar conditions were used for the AGG spectra except that a single data set was collected during 10 h with 1.2 ms contact time, 128 $t_1$ points, 65 kHz decoupling, and a recycle delay of 1.5 s.

To obtain exchange spectra, four FIDs were taken at each $t_1$ value. Each of the FIDs, labeled as F($\tau$, Re), F($\tau$, Im), F($t_1 + \tau$, Re), or F($t_1 + \tau$, Im), was characterized by: (1) having either the $\tau$ or the $t_1 + \tau$ time as an integral number of rotor periods; and (2) containing either the real (Re) or imaginary (Im) component of magnetization in $t_1$. Hypercomplex data were generated in HSS processing with the expressions:

$$\begin{aligned} F_{HSS,Re} &= F(\tau, Re) + iF(\tau, Im) \\ &\quad + F(t_1 + \tau, Re) - iF(t_1 + \tau, Im) \end{aligned} \tag{10a}$$

$$\begin{aligned} F_{HSS,Im} &= -iF(\tau, Re) + F(\tau, Im) \\ &\quad + iF(t_1 + \tau, Re) + F(t_1 + \tau, Im) \end{aligned} \tag{10b}$$

and the corresponding data were obtained in HRG processing with the expressions:

$$\begin{aligned} F_{HRG,Re} &= F(\tau, Re) - iF(\tau, Im) \\ &\quad + F(t_1 + \tau, Re) + iF(t_1 + \tau, Im) \end{aligned} \tag{11a}$$

$$\begin{aligned} F_{HRG,Im} &= iF(\tau, Re) + F(\tau, Im) \\ &\quad - iF(t_1 + \tau, Re) + F(t_1 + \tau, Im). \end{aligned} \tag{11b}$$

The theory behind these formulas has been previously described in detail (Kentgens et al., 1987; Hagemeyer et al., 1989; Luz et al., 1992; Tycko et al., 1996; Tycko and Berger, 1999). The HSS and HRG FIDs were transformed into their respective 2D spectra using standard methods for hypercomplex data and NMRPipe software (States et al., 1982; Delaglio et al., 1995).

Line broadening was 150 Hz for the melittin and FP23 samples and either 50 Hz or 350 Hz for the AGG sample. The intrasite and intersite crosspeaks were resolved for melittin but not for FP23. For the AGG sample, the crosspeaks were resolved with 50 Hz line broadening and unresolved with 350 Hz line broadening.

For the melittin and FP23 samples, integrated crosspeak intensities were calculated by summing the intensities of nine points enclosed by a 150 Hz $\times$ 150 Hz area. For the AGG spectra processed with 50 Hz line broadening, the integrated intensities were calculated by summing the intensities of nine points enclosed by a 75 Hz $\times$ 75 Hz area. For AGG spectra processed with 350 Hz line broadening, the integrated intensities were calculated by summing the intensities of 169 points enclosed by a 325 Hz $\times$ 325 Hz area.

In addition to their dependence on $\varphi$ and $\psi$, the simulated intersite intensities depend on the orientation of the carbonyl CSA principal axes relative to the carbonyl chemical bonds and on the carbonyl CSA principal values. The former were taken from the literature with the following orientations: $\delta_{33}$ perpendicular to the peptide plane and $\delta_{22}$ at an angle $\chi = 130°$ from the C-N bond (Oas et al., 1987). The CSA principal values were experimentally determined from measurements of the 1D peak spinning sideband intensities measured at a few different spinning frequencies between 2 kHz and 4 kHz (Herzfeld and Berger, 1980). The effect of $^{13}$C-$^{14}$N dipolar coupling was taken into account in the principal value determination. For melittin, the individual site spinning sideband intensities were derived from deconvolution of each experimental spinning sideband into two Gaussian peaks. The best-fit Gly-3 and Ala-4 $\delta_{11}$, $\delta_{22}$, $\delta_{33}$ CSA principal values are 239, 189, 91 ppm and 242, 198, 92 ppm, respectively. For FP23 the unresolved CSA principal values are 241, 179, 93 ppm. For resolved AGG sites, the Ala-1 and Gly-2 principal values are 245, 186, 88 ppm and 242, 182,

89 ppm (Weliky and Tycko, 1996). Analysis of a 1D AGG spectrum at 2.5 kHz spinning speed with 350 Hz line broadening yielded unresolved resonances with a single set of principal values 243, 182, 91 ppm. The experimental uncertainty of each principal value is ±2 ppm. Simulated 2D SSRS-MASE AGG spectra were generated using both the resolved and the unresolved principal values.

Although the anisotropic local field experienced by the labeled carbonyl is dominated by the CSA, the smaller but well-understood $^{13}C$– $^{14}N$ dipolar coupling also contributes to the field. Using the observation that the $^{14}N$ longitudinal relaxation is longer than $t_1$ or $t_2$ but shorter than $\tau$ (Weliky and Tycko, 1996), the $^{13}C$–$^{14}N$ coupling was incorporated into the calculation of simulated HSS or HRG intersite intensities with a sum of nine equally weighted components, each of which had a particular $^{14}N$ azimuthal quantum number in $t_1$ and an uncorrelated $^{14}N$ azimuthal quantum number in $t_2$.

Finally, in the case of unresolved crosspeaks, it is necessary to subtract the intrasite intensity from the experimental crosspeak intensity before fitting the remaining intersite intensity. The intrasite contribution was calculated using our knowledge of the number of labeled and natural abundance carbonyls in the sample.

The simulated spectral intensities were compared to experimental integrated peak intensities using the $\chi^2$ metric:

$$\chi^2(\varphi, \psi) = \sum_j \left\{E_j - \left[\lambda(\varphi, \psi) \times S_j(\varphi, \psi)\right]\right\}^2/\sigma^2 \quad j = 1 \text{ to } N, \tag{12}$$

where $E_j$ and $S_j(\varphi, \psi)$ are experimental and simulated off-diagonal crosspeak intensities, $\sigma^2$ is the mean-squared uncertainty per data point, $\lambda(\varphi, \psi)$ is a scaling factor fitted to minimize $\chi^2$ at each $(\varphi, \psi)$ pair, and N is the total number of data points. Equation 12 is equivalent to Equation 1 except that $y_j^{expt.}$ is replaced by $E_j$ and $y_j^{calc.}$ is replaced by $\lambda(\varphi, \psi) \times S_j(\varphi, \psi)$. Because mirror image (across-the-diagonal) crosspeaks always have the same simulated intensity, the experimental mirror image crosspeak intensities were summed. Thus, for a 5 × 5 2D spectral array of spinning sidebands, the forty (resolved) or twenty (unresolved) off-diagonal crosspeak intensities were reduced to twenty or ten data points. A few representative fits were also done without summing and were similar to those with summed data.

It was assumed that the most likely $(\varphi, \psi)$ were those at $\chi^2$ minima and there was a two-step process for finding these minima. First, $\lambda$ was uniquely obtained for each $(\varphi, \psi)$ using linear fitting that minimized $\chi^2$ at each $(\varphi, \psi)$ pair. Second, because $S_j(\varphi, \psi)$ is nonlinear in $\varphi$ and $\psi$, $\chi^2$ was calculated at a large number of points in the total grid of possible $(\varphi, \psi)$ values and $\chi^2$ minimum locations were identified by visual inspection of contour plots of $\chi^2$ vs. $\varphi$ and $\psi$. The points in the $(\varphi, \psi)$ grid were separated by 5° increments in the ranges $-180° \le \varphi \le 0°$ and $-180° \le \psi \le 180°$. These ranges cover the entire Ramachandran plot because the simulated crosspeak intensity pattern for a $(\varphi, \psi)$ pair is the same as for its mirror image pair $(-\varphi, -\psi)$. For residues other than glycine, steric considerations often imply that one of the pairs is highly improbable (Cantor and Shimmel, 1980).

For the membrane-bound peptide spectra, the value of $\sigma^2$ in Equation 12 was set to be the instrumental noise, or more precisely twice the mean-squared deviation of a set of spectral intensities measured near but not on the array of exchange crosspeaks. The factor of two was included because each data point is the sum of mirror-image crosspeak intensities. For AGG, uncertainty in the simulated intensities also made a significant contribution to the total uncertainty and this simulation uncertainty was incorporated into the analyses by a method described in the Results section.

Because the HSS and HRG spectra contain independent information, their fitting results were combined to improve discrimination between the $\chi^2$ minima. First, $\chi^2$ was calculated for each spectrum and then $\chi^2_{sum} = \chi^2_{HSS} + \chi^2_{HRG}$ was calculated at each $(\varphi, \psi)$. Because the sum of two $\chi^2$ distributions is again a $\chi^2$ distribution, we can apply the $\Delta\chi^2$ method described in the Theory section to $\chi^2_{sum}$. The validity of the overall approach is supported by the finding that for both resolved and unresolved AGG spectra, the $(\varphi, \psi)$ conformation at the global minimum $\chi^2_{sum}$ is very close to the correct structure.

## Results

### *1D spectra*

The 1D $^{13}C$ CP-MAS spectra for the AGG, melittin, and FP23 samples are displayed in Figure 1. For the AGG spectra in (a), processing was done with 25 Hz (top) and 350 Hz (bottom) line broadening. The isotropic chemical shifts of the Ala-1 and Gly-2 carbonyls are 173 and 171 ppm, respectively (Weliky

*Table 1.* $\chi^2$ Minima in fits of 2D SSRS-MASE data for melittin and FP23

| Sample | Processing | Figure | $\chi^2$ [a] | φ, ψ (°) |
|---|---|---|---|---|
| | HSS | 2c | 18 | −45, −35 |
| | | | 19 | −50, −120 |
| | | | 19 | −110, −35 |
| Melittin:DTPC | | | 22 | −120, 145 |
| | | | 23 | −125, 95 |
| | HRG | 2d | 10 | −85, −45 |
| | | | 12 | −60, −45 |
| | Sum | 2e | 35 | −85, −45 |
| | | | 38 | −60, −45 |
| | HSS | 3c | 7 | −130, 130 |
| | | | 12 | −65, −105 |
| | | | 13 | −50, −40 |
| | HRG | 3d | 5 | −105, −70 |
| | | | 5 | −60, −105 |
| | | | 5 | −100, 110 |
| FP23:DTPC | | | 9 | −75, 95 |
| | | | 11 | −30, −100 |
| | | | 11 | −90, 65 |
| | Sum | 3e | 17 | −60, −105 |
| | | | 17 | −120, 105 |
| | | | 18 | −100, −70 |
| | | | 25 | −30, −100 |

[a]The $\chi^2$ values were calculated with the $\sigma^2$ uncertainty based on the experimental spectral noise.

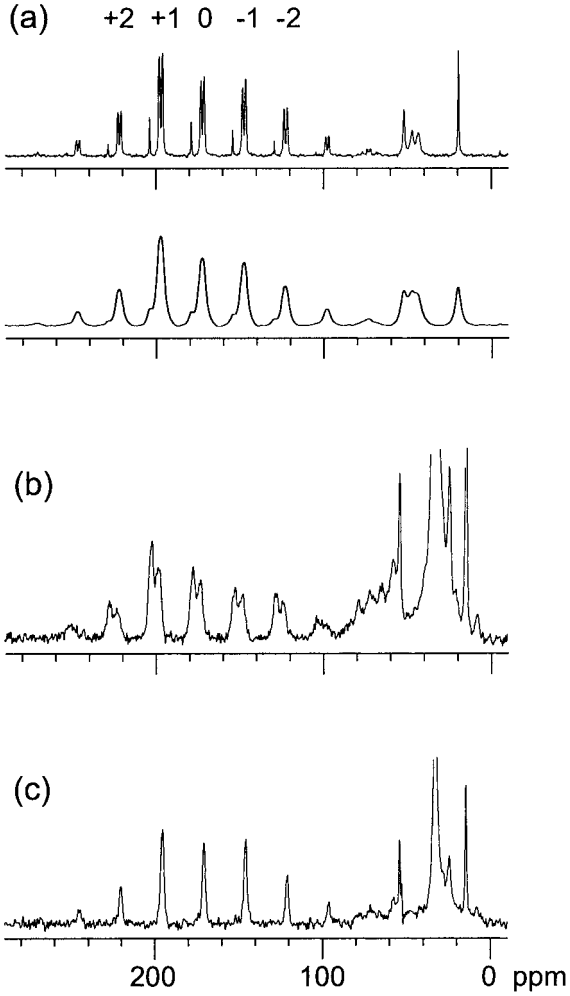


*Figure 1.* One-dimensional $^{13}$C CP-MAS spectra of (a) AGG, (b) melittin:DTPC, and (c) FP23:DTPC. The melittin and FP23 samples had a peptide:lipid mol ratio of 1:20. All spectra were taken at 2.5 kHz spinning frequency and the spinning sideband numbers between −2 and +2 are marked. The top spectrum in (a) and the spectra in (b) and (c) were processed with 25 Hz line broadening. The bottom spectrum in (a) was processed with 350 Hz line broadening. In (a), (b), and (c), the number of transients was 64, 4800, and 5600, respectively. In (b) and (c), the top of the lipid methylene resonance is truncated.

and Tycko, 1996). The inherent carbonyl linewidths for AGG are ∼ 1 ppm and contain some contribution from residual $^{13}$C-$^{14}$N dipolar couplings (Hexem et al., 1982). 25 Hz line broadening was used for the membrane-bound melittin and FP23 spectra displayed respectively in (b) and (c). The isotropic shifts of the melittin Gly-3 and Ala-4 carbonyls are 173 and 177 ppm, respectively, and the isotropic shift of the FP23 Leu-7 and Phe-8 carbonyls is 171 ppm. The linewidths for melittin and FP23 are ∼ 3 ppm and ∼ 2 ppm, respectively, which represent reasonably structured although not crystalline conformational distributions (Yang et al., 2001b).

### *2D spectra and analyses of membrane-bound peptides*

Figure 2 displays 2D SSRS-MASE spectra of the melittin sample processed by (a) HSS and (b) HRG methods and the corresponding fits in (c) and (d). The sum fit is displayed in (e) and Table 1 lists the $\chi^2$ minima. In general, the HRG fit is more strongly constrained than the HSS fit, and the sum fit closely resembles the HRG fit with a global minimum at (−85°, −45°) and a local minimum at (−60°, −45°) with $\Delta_e\chi^2 = 3$. Both of these minima correspond to helical structure at Ala-4 and are consistent with previous observations of an overall helical conformation of this membrane-bound peptide (Dempsey, 1990; Smith et al., 1994; Bechinger, 1997).

*Table 2.* $\chi^2$ minima in fits of 2D SSRS-MASE data for AGG

| Spectrum[a] | CSA PV[b] | Processing | Figure | $\chi^2$ [c] | φ, ψ (°) |
|---|---|---|---|---|---|
| Resolved | Resolved | HSS | 4c | 17 (90) | −90, 170 |
| | | | | 19 (100) | −95, −130 |
| | | HRG | 4d | 17 (104) | −95, 165 |
| | | | | 24 (149) | −95, −130 |
| | | Sum | 4e | 40 | −95, 165 |
| | | | | 43 | −95, −130 |
| Unresolved | Resolved | HSS | 4h | 7 (22) | −65, 165 |
| | | | | 9 (29) | −170, 65 |
| | | | | 13 (43) | −105, 165 |
| | | | | 13 (43) | −170, 110 |
| | | HRG | 4i | 7 (65) | −135, −95 |
| | | | | 7 (66) | −90, −135 |
| | | | | 7 (68) | −175, 100 |
| | | | | 8 (76) | −100, 165 |
| | | Sum | 4j | 22 | −100, 165 |
| | | | | 27 | −175, 100 |
| | | | | 27 | −75, 170 |
| Unresolved | Unresolved | HSS | 4k | 7 (38) | −105, 165 |
| | | | | 8 (42) | −170, 110 |
| | | | | 8 (44) | −65, 160 |
| | | | | 9 (52) | −170, 65 |
| | | HRG | 4l | 7 (31) | −150, −90 |
| | | | | 8 (34) | −135, −95 |
| | | | | 12 (50) | −90, −135 |
| | | | | 12 (52) | −175, 100 |
| | | | | 12 (52) | −80, −180 |
| | | | | 14 (59) | −100, 165 |
| | | Sum | 4m | 21 | −100, 165 |
| | | | | 24 | −175, 100 |
| | | | | 28 | −80, 175 |

[a]For resolved spectra, 50 Hz line broadening was applied. For unresolved spectra, 350 Hz line broadening was applied.

[b]Chemical shift anisotropy principal values. Fitting was based on simulated spectra calculated with CSA PV which were either distinct for the two carbonyl sites (resolved) or the same for the two sites (unresolved).

[c]The $\chi^2_n$ value is followed by the $\chi^2_u$ value in parentheses. As described in the text, the $\chi^2_u$ values only consider the experimental noise contribution to $\sigma^2$ while the $\chi^2_n$ values also consider the simulation uncertainty contribution to $\sigma^2$. The $\chi^2$ values for the sum fits are obtained by summing $\chi^2_n$ from HSS and HRG fits.

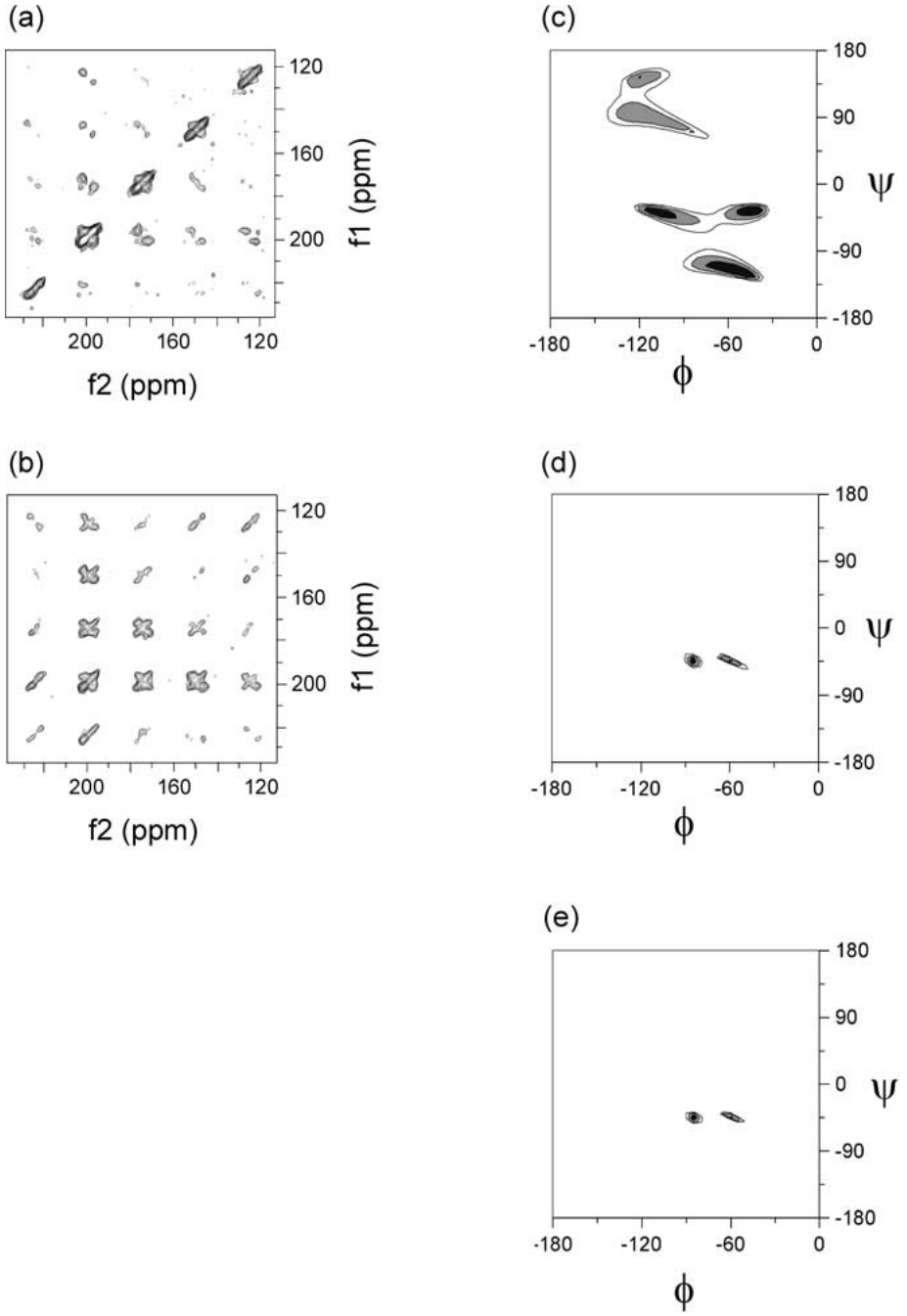


*Figure 2.* Two-dimensional SSRS-MASE spectra and least-squares fits of melittin:DTPC. The (a) HSS and (b) HRG spectra were processed with 150 Hz line broadening in each dimension. The corresponding $\chi^2$ fits are presented in (c) and (d). For these fits, the uncertainty was dominated by experimental noise. The fit in (e) is the sum of (c) and (d). In (c), (d), and (e), the darkest regions represent $\chi^2$ between 18 and 22, 10 and 14, and 35 and 39, respectively. Each increasingly lighter contour represents an increment of four units of $\chi^2$.

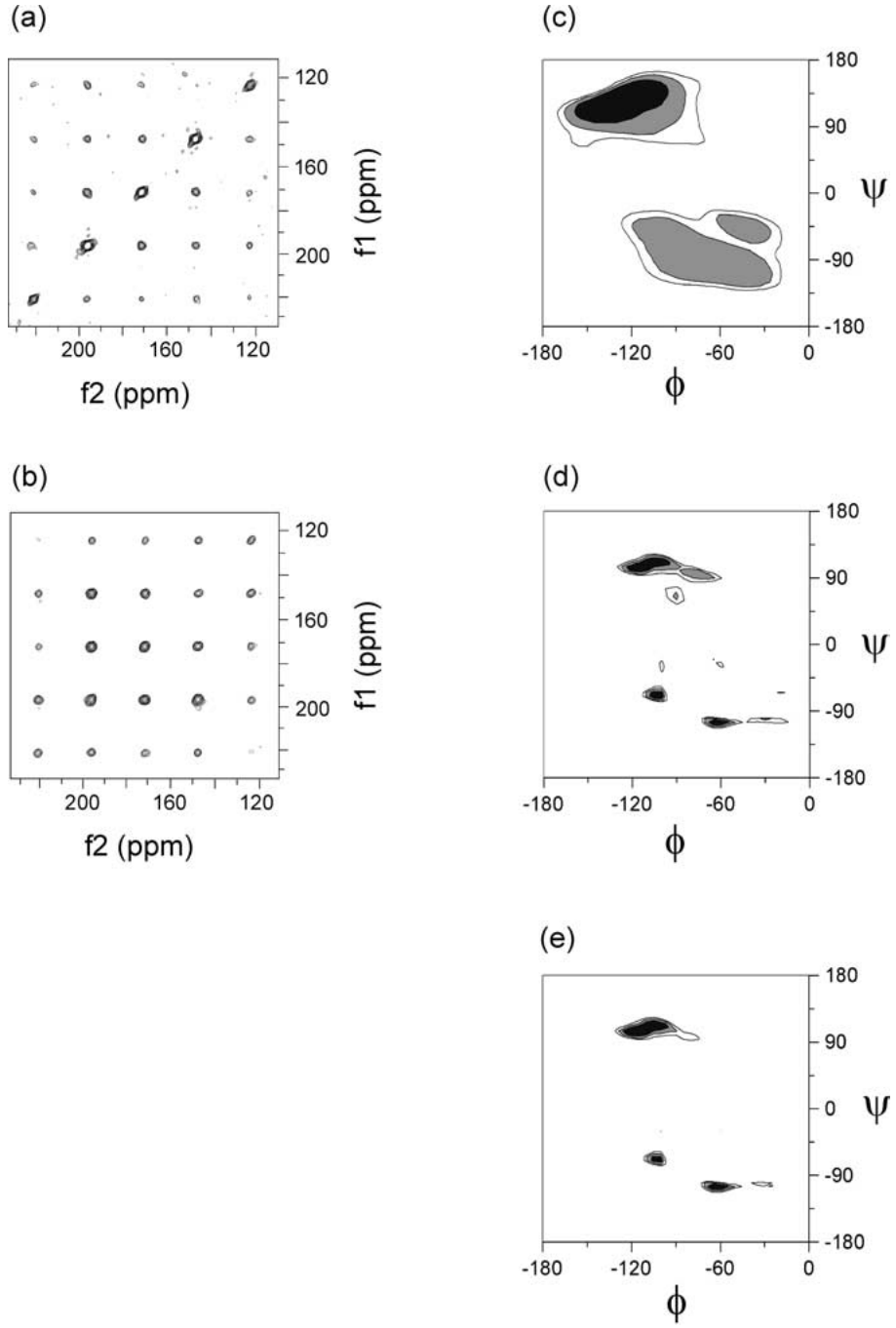


*Figure 3.* Two-dimensional SSRS-MASE spectra and least-squares fits of FP23:DTPC. The (a) HSS and (b) HRG spectra were processed with 150 Hz line broadening in each dimension. The corresponding $\chi^2$ fits are presented in (c) and (d). For these fits, the uncertainty was dominated by experimental noise. The fit in (e) is the sum of (c) and (d). In (c), (d), and (e), the darkest regions represent $\chi^2$ between 7 and 11, 5 and 9, and 17 and 21, respectively. Each increasingly lighter contour represents an increment of four units of $\chi^2$.

Figure 3 displays 2D SSRS-MASE NMR spectra of the FP23 sample processed by (a) HSS and (b) HRG methods and the corresponding fits in (c) and (d). The sum fit is displayed in (e) and Table 1 lists the $\chi^2$ minima. The sum fit has three minima within one unit of $\chi^2$ of each other and with ($\varphi$, $\psi$) values of ($-60°$, $-105°$), ($-120°$, $105°$), and ($-100°$, $-70°$). The unresolved Leu-7/Phe-8 chemical shift of 171.2 ppm is consistent with β strand structure at Phe-8, which suggests that the ($-120°$, $105°$) conformation in the sum fit is the correct one (Wishart et al., 1991; Yang et al., 2001a).

As described in the Theory section, it is most likely that the correct structure will be near the global $\chi^2$ minimum conformation or near a local $\chi^2$ minimum conformation which has $\Delta_e\chi^2 < 4$. Therefore, in Figures 2 and 3, the darkest regions correspond to $\Delta_e\chi^2 < 4$. Additional displayed regions with $4 < \Delta_e\chi^2 < 8$, and $8 < \Delta_e\chi^2 < 12$ are less likely to include the correct structure. Because $\Delta_e\chi^2$ is used in this quantitative manner, it is of some importance to know $\sigma^2$ accurately so that the $\chi^2$ and $\Delta_e\chi^2$ are correctly calculated. For the membrane-bound peptides, $\sigma^2$ was calculated solely from spectral noise, because it appeared that simulation uncertainty had minimal impact on the fits. For example, HSS and HRG fits based on different but reasonable simulation parameter values (e.g. CSA principal values) showed relatively small ($\leq 4$) variations in the $\Delta_e\chi^2$ values and only small ($\leq 10°$) variations in the ($\varphi$, $\psi$) values at the $\chi^2$ minima. In addition, the HSS and HRG fits in Figures 2 and 3 had global minimum $\chi^2$ values which were close to $\nu$, the number of degrees of freedom in the analysis. This result is significant because for the correct structure, correct fitting function, and correct value of $\sigma^2$, the most probable value of $\chi^2$ should be about equal to $\nu$ (Arley and Buch, 1966; Bevington and Robinson, 1992; Press et al., 1996). For fitting of resolved HSS or HRG spectra, $\nu = 17$, and for unresolved spectra, $\nu = 7$, as calculated from the difference between the number of data points (20 or 10) and the number of fitted parameters (3 for $\lambda$, $\varphi$, $\psi$). When HSS and HRG fits are summed, the value of $\nu$ is doubled to 34 or 14.

*2D spectra and analyses of AGG*

Figure 4 displays the 2D SSRS-MASE spectra and fits of AGG and Table 2 lists the $\chi^2$ minima. In Figures 4a and b, the spectra were processed by the HSS and HRG methods, respectively, and with 50 Hz line broadening in each dimension. $\chi^2$ fits of the HSS and HRG spectra are displayed in (c) and (d), respectively, and are based on simulations which used the resolved Ala-1 and Gly-2 CSA principal values. The sum fit is displayed in (e). The global minimum of the sum fit lies at ($-95°$, $165°$), which is close to the structure of ($-83°$, $170°$) obtained by neutron diffraction (Subramanian and Lalitha, 1983; Lalitha et al., 1985).

Spectra (f) and (g) represent HSS- and HRG-processed AGG spectra, respectively, which were unresolved because of 350 Hz line broadening in each dimension. The $\chi^2$ contour plots in (h) and (k) are fits of spectrum (f) using simulations based on resolved and unresolved principal values, respectively, while the plots in (i) and (l) are the corresponding fits of spectrum (g). The (j) and (m) plots are the sum fits (h) + (i) and (k) + (l), respectively. Both of the sum fits have similar appearance, indicating that they are robust with respect to uncertainty in CSA principal values, and each has its global $\chi^2$ minimum at ($-100°$, $165°$) which is close to the correct structure. These results demonstrate that 2D SSRS-MASE analysis provides accurate structural information when the labeled sites have unresolved chemical shifts and when unresolved CSA principal values are used in the simulations. These results are significant because many membrane-bound peptides have unresolved carbonyl chemical shifts.

As with the fits of membrane-bound peptides, there are multiple $\chi^2$ minima in the AGG fits which have significantly different conformations. Because the ($\varphi$, $\psi$) values of $\chi^2$ minimum conformations can be different in HSS and HRG processing, the sum fits are useful in discriminating against incorrect structures. It is visually apparent that the sum fits in (j) and (m) constrain the conformation more strongly to its correct value than the individual HSS and HRG fits in (h), (i), (k), and (l).

*Simulation uncertainty in AGG analyses*

For AGG, we first calculated $\chi^2$ using a $\sigma^2$ value based only on spectral noise. The resulting values of $\chi^2$, denoted '$\chi^2_u$', are listed in parentheses in Table 2. However, two lines of evidence suggested that $\sigma^2$ also contained a significant contribution from simulation uncertainty. First, we observed that the $\chi^2_u$ values at the global minima were always significantly higher than $\nu$, which is statistically highly unlikely if we were treating uncertainty correctly. Unreasonably large $\chi^2_u$ values were also observed in previous 2D SSRS-MASE studies of AGG which used a different console, pulse programming language, and probe, so

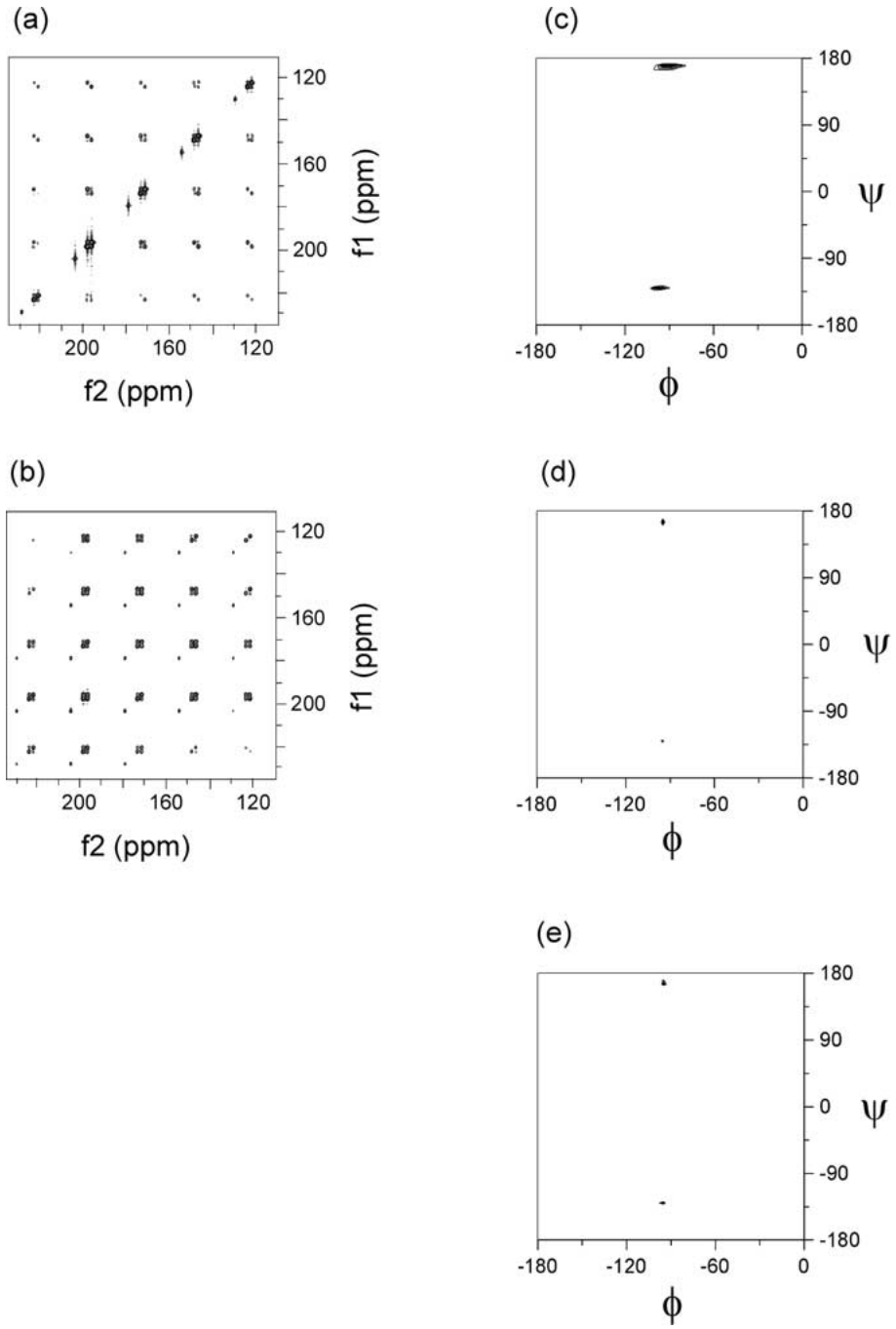


*Figure 4.* Two-dimensional SSRS-MASE spectra and least-squares fits of polycrystalline AGG. The correct AGG structure lies at (−83°, 170°). The resolved (a) HSS and (b) HRG spectra were processed with 50 Hz line broadening in each dimension. The accompanying $\chi^2$ fits are displayed in (c) and (d). The fit in (e) is the sum of (c) and (d). The unresolved (f) HSS and (g) HRG spectra were processed with 350 Hz line broadening in each dimension. The accompanying $\chi^2$ fits for the HSS spectrum are displayed in (h) and (k) and the $\chi^2$ fits for the HRG spectrum are displayed in (i) and (l). The (h), (i) fits were based on simulations which used resolved Ala-1 and Gly-2 CSA principal values while the (k), (l) fits were based on simulations which used a single set of unresolved principal values for both sites. The fit in (j) is the sum of the (h) and (i) fits and the fit in (m) is the sum of the (k) and (l) fits. In the fits, the darkest region represents $\chi^2$ between the following values: (c), (d), 17–21; (e), 40–44; (h), (i), (k), (l), 7–11; (j), 22–26; and (m) 21–25. For all fits, each increasingly lighter contour represents an increment of four units of $\chi^2$.

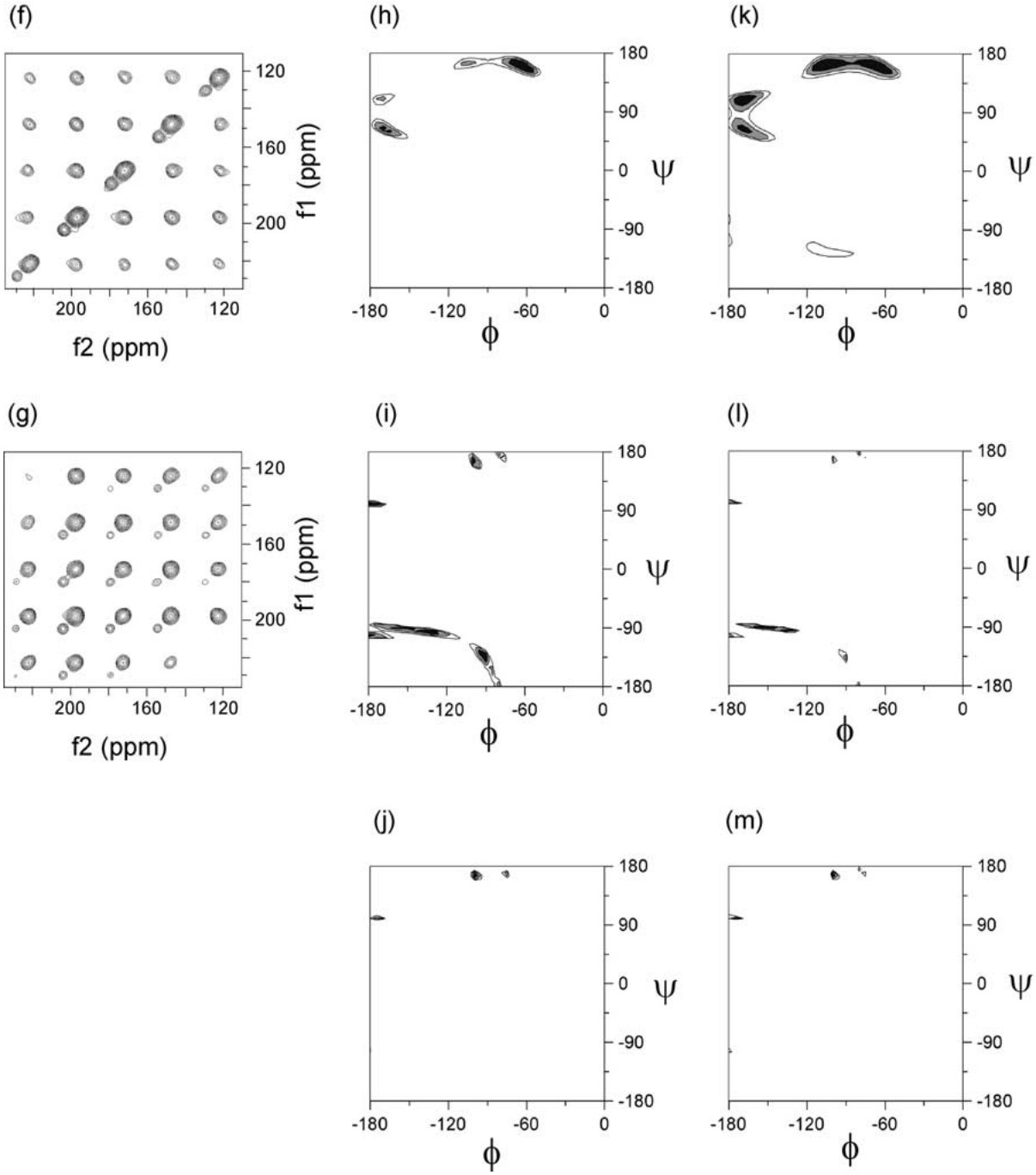


*Figure 4.* Continued.

it is unlikely that these values were due to a problem specific to our experimental setup (Tycko and Berger, 1999). Additional evidence for simulation uncertainty was found in HSS or HRG fits based on different but reasonable simulation input parameter values (e.g. CSA principal values and/or $\chi$ angles). Comparison of the simulations showed variations in $\Delta_e\chi_u^2$ which were much larger than four, which is unlikely if the uncertainty were dominated by experimental noise. For example, when unresolved HSS spectra were fit with either resolved or unresolved principal values, $\Delta_e\chi_u^2$ for the mimima ($-65°$, $165°$) and ($-105°$, $165°$) changed from 21 to $-6$ (cf. Table 2). Significantly, the simulation-induced variations in ($\varphi$, $\psi$) values at minima were small ($\leq 10°$ and typically $0°$ or $5°$).

We incorporated simulation uncertainty into the AGG analysis by considering it as a random error which contributes to $\sigma^2$. The magnitude of its contribution is not known very accurately, so we used an empirical approach in which $\sigma^2$ in Equation 12 was set so that the global minimum $\chi^2$ equals $\nu$. The reasoning for this choice is that for the correct structure, correct fitting function, and correct value of $\sigma^2$, the most probable value of $\chi^2$ should be approximately equal to $\nu$. Table 2 lists these '$\chi_n^2$' minima values and $\chi_n^2$ is also plotted in the HSS and HRG fits in Figure 4. The $\chi_{sum}^2$ values listed in Table 2 are calculated using $\chi_n^2$ values and the fits in (j) and (m) are the sums of the $\chi_n^2$ fits. The fitting plots in (h–j) and in (k–m) are based on different simulation input parameters and the similarity between corresponding plots (e.g., (j) and (m)) is evidence that the $\chi_n^2$ approach is a reasonable method to treat simulation uncertainty. The large contribution of simulation uncertainty in the AGG fitting but not in the membrane peptide fitting is likely a result of the much higher signal-to-noise and the corresponding smaller experimental uncertainty in the AGG data.

*Fitting robustness*

Since the 2D SSRS-MASE analysis relies on accurate measurement of experimental crosspeak intensities and accurate simulation of these intensities, a systematic investigation was made of the dependence of the fitting on spectral processing parameters (baseline correction, phasing, and integration width) and simulation parameters (intrasite intensity, CSA principal values, and CSA $\chi$ angles). In these analyses, principal values were changed by $\pm 2$ ppm and $\chi$ angles were changed by $\pm 5°$, which are the approximate uncertainties in these parameters (Oas et al., 1987). Intrasite intensity was varied between 80% and 120% of its correct value. We focused on sum fits because they provided the greatest information about peptide structure. These analyses were carried out on both membrane peptide and AGG data and yielded two main conclusions. First, use of different but reasonable choices of processing or simulation parameters caused little change in the ($\varphi$, $\psi$) values at $\chi_{sum}^2$ minima. More specifically, comparison of twenty different membrane peptide fits showed an average variation of $1.8°$ in $\varphi$ or $\psi$, and comparison of twenty-six different AGG fits showed an average variation of $1.6°$ in $\varphi$ or $\psi$. Second, the changes in $\Delta_e\chi_{sum}^2$ values were typically less than four, which is the approximate $\Delta_e\chi^2$ significance range derived in the Theory section. In particular, variation of processing and simulation parameters yielded an average change in $\Delta_e\chi_{sum}^2$ of $1.8 \pm 1.7$ for the membrane peptides and $5.9 \pm 7.0$ for AGG. In AGG fitting, the largest $\Delta_e\chi_{sum}^2$ changes were detected with variation of the CSA $\chi$ angles; when $\chi$ angle variation was not included, the average change in AGG $\Delta_e\chi_{sum}^2$ was only $2.8 \pm 2.5$. Relative to membrane peptides, the larger dependence of the AGG $\Delta_e\chi_{sum}^2$ on simulation parameters is consistent with the larger relative contribution of simulation uncertainty in the AGG fitting.

## Discussion

Membrane-bound peptides and proteins are important biological systems, but it is difficult to study their structures in native membrane environments by crystallographic or solution NMR methods. Thus, they represent an important niche for solid state NMR methodologies. The solid state NMR spectra of membrane-bound peptides typically have low signal-to-noise ratios because of $\leq 2$ $\mu$mol sample quantities and 1–3 ppm linewidths. Therefore, in order to obtain greater signals, it is often advantageous to use larger volume ($\geq$ 200 $\mu$l) rotors, which have the disadvantages of reduced decoupling fields, RF homogeneity, and MAS frequencies. 2D SSRS-MASE is not sensitive to these parameters and our main result is that the method provides accurate local conformational constraints for membrane peptides in these large rotors.

*Conformations of melittin and FP23*

The two membrane-bound peptides under study, melittin and FP23, both interact strongly with membranes but are shown in our work to likely have different local conformations ($\alpha$ helical and $\beta$ strand,

respectively) in the labeled regions. For melittin, the conformational data were consistent with previous infrared, electron spin resonance, and NMR results of an overall helical conformation (Dempsey, 1990; Smith et al., 1994; Bechinger, 1997). For FP23, a β strand structure is consistent with the carbonyl chemical shift and with the preponderance of previous evidence suggesting an overall β conformation at 1:20 peptide:lipid mol ratio (Durell et al., 1997; Yang et al., 2001a). At lower peptide:lipid mol ratios in particular lipid compositions, some investigators have also observed helical structure (Martin et al., 1996; Durell et al., 1997; Gordon et al., 2002; Saez-Cirion and Nieva, 2002; Bodner and Weliky, unpublished data). The β strand structure which we observe would be consistent with formation of a β sheet structure composed of oligomerized peptides. Such oligomerization has been postulated as a structural requirement for fusion peptide-induced membrane fusion (Kliger et al., 1997; Pereira et al., 1997; Curtain et al., 1999), and investigation of FP23 oligomer structure is currently underway in our laboratory.

*General applicability of dual processing*

Tycko et al. previously demonstrated the greater information obtained using HSS and HRG dual processing of resolved 2D SSRS-MASE AGG data (Tycko and Berger, 1999). Our work extends the utility of dual processing in several ways. First, sum fitting was shown for resolved AGG spectra to be an accurate and useful means of combining the results from the two processing methods (Bennett et al., 1998b; Weliky et al., 1999; Balbach et al., 2000). Second, for membrane-bound melittin, sum fitting was shown to provide greater conformational constraints than HSS processing. Third, sum fitting was shown to work even when there are unresolved chemical shifts. An important part of this third result was that the HRG fits were relatively insensitive to the magnitude of subtracted intrasite intensity over at least a ±20% range of its expected value. This observation is important for membrane peptides for which there can be some uncertainty in intrasite intensity because of uncertainty in the peptide:lipid ratio and because of the presence of carbonyl-containing ester-linked lipids.

*Accuracy of 2D SSRS-MASE in determining conformation*

The accuracy of 2D SSRS-MASE can be gauged by comparing the correct AGG structure at (−83°, 170°) to the (φ, ψ) values of sum fit $\chi^2$ minima which are near it. For the resolved spectra, the $\chi^2$ minimum at (−95°, 165°) is close to the correct structure while for the unresolved spectra, the $\chi^2$ minima at (−100°, 165°), (−75°, 170°), and (−80°, 175°) are all close to the correct structure. These results suggest an accuracy of about ±20° in φ and about ±5° in ψ. Variation of processing and simulation parameters for the fits of the melittin, FP23, and AGG spectra suggests a precision of about ±5° in the (φ, ψ) values at each $\chi^2$ minimum. For FP23, there are also significant regions surrounding each minimum which are reasonable fits to the data.

For both the AGG and FP23 samples, the sum fittings show $\chi^2$ minima whose (φ, ψ) values are significantly different than those at the global minima. The $\Delta_e\chi^2$ analysis is a reasonable approach for evaluating the likelihood that the local minimum structure is correct. In many cases, the $\Delta_e\chi^2$ differences are small enough that other information will be required to find the most probable structure. The carbonyl chemical shift can be useful (as it was for FP23) and it has also been useful to apply another structure determination methodology (usually multiple-pulse) for doubly carbonyl labeled peptides (Wishart et al., 1991). Possible methods include RFDR, DRAWS, and DQCSA techniques (Gregory et al., 1997; Bennett et al., 1998a; Bower et al., 1999; Blanco and Tycko, 2001). By combining the results of these methods, it is sometimes possible to constrain the peptide to a single conformation (Bennett et al., 1998a; Weliky et al., 1999; Balbach et al., 2000).

*Comparison of 2D SSRS-MASE with other structural methodologies*

The general technical strengths of 2D SSRS-MASE for peptide conformational measurements are: (1) Use of slow spinning frequencies; (2) sparseness of pulses and insensitivity to RF inhomogeneity; (3) insensitivity to $^1$H decoupling field; (4) accuracy and robustness of the fitting; and (5) use of widely available and inexpensive 1-$^{13}$C labeled amino acids. In addition, the 2D and slow spinning aspects provide for multiple crosspeaks (i.e., data points) which lead to strong constraints on both φ and ψ. On the other hand, these latter aspects also degrade the sensitivity of 2D SSRS-MASE with respect to quasi-1D structural methods such as multiple-pulse techniques which probe intercarbonyl dipolar coupling. By 'quasi-1D', we mean acquisition of several 1D spectra with different parameter values (e.g., dephasing times). In a few cases, 2D SSRS-MASE has been done in conjunc-

tion with a RFDR-based dipolar recoupling method and 2D SSRS-MASE appeared to require about 1.5–3 times more signal averaging time than RFDR (Bennett et al., 1998a; Weliky et al., 1999; Balbach et al., 2000). However, the conformational constraints of 2D SSRS-MASE were much better defined than those of the RFDR method. Relative to 2D SSRS-MASE, the experimental sensitivity and simulation accuracy of multiple-pulse methods typically have a greater dependence on RF inhomogeneity and $^1$H decoupling field.

*Uncertainty in 2D SSRS-MASE analysis*

For 2D SSRS-MASE analysis, our study presents evidence that there are both experimental and simulation contributions to the overall fitting uncertainty. For membrane peptides, the experimental signal-to-noise will usually be low enough that the overall uncertainty is dominated by the spectral noise. Hence, longer signal averaging time will lower uncertainty and will result in improved discrimination between $\chi^2$ minima as well as tighter constraints on the conformation at a particular minimum. For pure solid peptides such as AGG, the signal-to-noise can be high enough that simulation uncertainty is also an important factor in the $\chi^2$ analysis. In this case, longer signal averaging time will not improve discrimination between $\chi^2$ minima. This result should be considered when applying 2D SSRS-MASE to structurally interesting solid peptides such as those which form fibrils (Lansbury et al., 1995; Benzinger et al., 1998; Balbach et al., 2000) and to solid proteins such as elastin (Hong et al., 2002; Perry et al., 2002).

## Conclusions

2D SSRS-MASE spectroscopy was applied to provide constraints on local secondary structure of two peptides which interact with membranes. One of these peptides, melittin, is the major component of bee venom and has hemolytic activity while the other peptide, FP23, is derived from the HIV-1 gp41 fusion protein and is the most critical domain for viral/target cell membrane fusion. In the conformational analyses, the linearly independent HSS and HRG data processing schemes were applied to each data set and the resulting fits were summed to provide the greatest conformational information. The sum fits were consistent with a best-fit α helical structure for membrane-bound melittin at its Ala-4 residue and a good-fit β strand structure for membrane-bound FP23 at its Phe-8 residue. The melittin analysis is consistent with the known overall helical peptide structure, and the FP23 structure is consistent with the carbonyl chemical shift and with results from other biophysical studies.

The accuracy and robustness of the 2D SSRS-MASE analysis was further explored through studies of polycrystalline AGG, a peptide of known structure. It was shown that the method has high accuracy for peptides with unresolved carbonyl resonances. Further methodological work on melittin, FP23, and AGG demonstrated the robustness of the analysis to reasonable variation of processing parameters, CSA principal values and χ angles, and magnitude of intrasite crosspeak intensity. For high signal-to-noise experimental data, an empirical method was introduced to account for the impact of simulation uncertainty on the data analysis.

The fitting of 2D SSRS-MASE data often results in local $\chi^2$ minima whose conformations are very different from the global minimum conformation. We derived an approximate formula, $\Delta_e\chi^2/\sigma_{\Delta\chi^2} \approx \sqrt{\Delta_e\chi^2}/2$, to semi-quantitatively assess differences in $\chi^2$ between the minima. Application of this formula suggests that $\Delta_e\chi^2$ differences $\leq 4$ do not have great significance. Although the $\Delta_e\chi^2/\sigma_{\Delta\chi^2}$ formula is specifically applied to interpretation of 2D SSRS-MASE data, it should be generally applicable to any data analysis for which least squares fitting yields multiple minima.

## Acknowledgements

We acknowledge Robert Tycko for useful discussions and for his CSA principal value and HSS simulation program. We acknowledge Andy Wijaya for help with simulations. D.P.W. acknowledges a Camille and Henry Dreyfus Foundation New Faculty Award and NIH AI47153.

## References

Arley, N. and Buch, K.R. (1966) *Introduction to the Theory of Probability and Statistics*, Wiley, New York.

Asakura, T., Ashida, J., Yamane, T., Kameda, T., Nakazawa, Y., Ohgo, K. and Komatsu, K. (2001) *J. Mol. Biol.*, **306**, 291–305.

Balbach, J.J., Ishii, Y., Antzutkin, O.N., Leapman, R.D., Rizzo, N.W., Dyda, F., Reed, J. and Tycko, R. (2000) *Biochemistry*, **39**, 13748–13759.

Bechinger, B. (1997) *J. Membr. Biol.*, **156**, 197–211.

Bennett, A.E., Rienstra, C.M., Griffiths, J.M., Zhen, W.G., Lansbury, P.T. and Griffin, R.G. (1998a) *J. Chem. Phys.*, **108**, 9463–9479.

Bennett, A.E., Weliky, D.P. and Tycko, R. (1998b) *J. Am. Chem. Soc.*, **120**, 4897–4898.

Benzinger, T.L., Gregory, D.M., Burkoth, T.S., Miller-Auer, H., Lynn, D.G., Botto, R.E. and Meredith, S.C. (1998) *Proc. Natl. Acad. Sci. USA*, **95**, 13407–13412.

Bevington, P.R. and Robinson, D.K. (1992) *Data Reduction and Error Analysis for the Physical Sciences*, McGraw-Hill, Boston.

Blanco, F.J. and Tycko, R. (2001) *J. Magn. Reson.*, **149**, 131–138.

Bower, P.V., Oyler, N., Mehta, M.A., Long, J.R., Stayton, P.S. and Drobny, G.P. (1999) *J. Am. Chem. Soc.*, **121**, 8373–8375.

Cantor, C.R. and Shimmel, P.R. (1980) *Biophysical Chemistry*, W.H. Freeman, New York.

Chang, C.D., Waki, M., Ahmad, M., Meienhofer, J., Lundell, E.O. and Haug, J.D. (1980) *Int. J. Peptide Protein Res.*, **15**, 59–66.

Creemers, A.F., Klaassen, C.H., Bovee-Geurts, P.H., Kelle, R., Kragl, U., Raap, J., de Grip, W.J., Lugtenburg, J. and de Groot, H.J. (1999) *Biochemistry,* **38**, 7195–7199.

Curtain, C., Separovic, F., Nielsen, K., Craik, D., Zhong, Y. and Kirkpatrick, A. (1999) *Eur. Biophys. J.*, **28**, 427–436.

Delaglio, F., Grzesiek, S., Vuister, G.W., Zhu, G., Pfeifer, J. and Bax, A. (1995) *J. Biomol. NMR,* **6**, 277–293.

Dempsey, C.E. (1990) *Biochim. Biophys. Acta*, **1031**, 143–161.

Durell, S.R., Martin, I., Ruysschaert, J.M., Shai, Y. and Blumenthal, R. (1997) *Mol. Membr. Biol.*, **14**, 97–112.

Edzes, H.T. and Bernards, J.P.C. (1984) *J. Am. Chem. Soc.*, **106**, 1515–1517.

Eilers, M., Reeves, P.J., Ying, W., Khorana, H.G. and Smith, S.O. (1999) *Proc. Natl. Acad. Sci. USA*, **96**, 487–492.

Freed, E.O., Delwart, E.L., Buchschacher Jr., G.L. and Panganiban, A.T. (1992) *Proc. Natl. Acad. Sci. USA*, **89**, 70–74.

Freed, E.O., Myers, D.J. and Risser, R. (1990) *Proc. Natl. Acad. Sci. USA*, **87**, 4650–4654.

Gordon, L.M., Mobley, P.W., Pilpa, R., Sherman, M.A. and Waring, A.J. (2002) *Biochim. Biophys. Acta-Biomembr.*, **1559**, 96–120.

Gregory, D.M., Mehta, M.A., Shiels, J.C. and Drobny, G.P. (1997) *J. Chem. Phys.*, **107**, 28–42.

Griffin, R.G. (1998) *Nat. Struct. Biol.*, **5 Suppl**, 508–512.

Hagemeyer, A., Schmidt-Rohr, K. and Spiess, H.W. (1989) *Adv. Magn. Reson.*, **13**, 85–130.

Henrichs, P.M. and Linder, M. (1984) *J. Magn. Reson.*, **58**, 458–461.

Herzfeld, J. and Berger, A.E. (1980) *J. Chem. Phys.*, **73**, 6021–6030.

Herzfeld, J., Roberts, J.E. and Griffin, R.G. (1987) *J. Chem. Phys.*, **86**, 597–602.

Hexem, J.G., Frey, M.H. and Opella, S.J. (1982) *J. Chem. Phys.*, **77**, 3847–3856.

Hirsh, D.J., Hammer, J., Maloy, W.L., Blazyk, J. and Schaefer, J. (1996) *Biochemistry,* **35**, 12733–12741.

Hong, M., McMillan, R.A. and Conticello, V.P. (2002) *J. Biomol. NMR*, **22**, 175–179.

Hoult, D.I. (1975) *Proc. Roy. Soc. London, Ser. A.*, **344**, 311–340.

Kentgens, A.P.M., Deboer, E. and Veeman, W.S. (1987) *J. Chem. Phys.*, **87**, 6859–6866.

Kliger, Y., Aharoni, A., Rapaport, D., Jones, P., Blumenthal, R. and Shai, Y. (1997) *J. Biol. Chem.*, **272**, 13496–13505.

Lalitha, V., Subramanian, E. and Bordner, J. (1985) *Indian J. Pure Appl. Phys.*, **23**, 506–508.

Lansbury, P.T., Jr., Costa, P.R., Griffiths, J.M., Simon, E.J., Auger, M., Halverson, K.J., Kocisko, D.A., Hendsch, Z.S., Ashburn, T.T., Spencer, R.G.S., Tidor, B. and Griffin, R.G. (1995) *Nat. Struct. Biol.*, **2**, 990–998.

Lapatsanis, L., Milias, G., Froussios, K. and Kolovos, M. (1983) *Synthesis-Stuttgart*, **8**, 671–673.

Long, H.W. and Tycko, R. (1998) *J. Am. Chem. Soc.*, **120**, 7039–7048.

Luz, Z., Spiess, H.W. and Titman, J.J. (1992) *Israel J. Chem.*, **32**, 145–160.

Martin, I., Schaal, H., Scheid, A. and Ruysschaert, J.M. (1996) *J. Virol.*, **70**, 298–304.

Metz, G., Wu, X.L. and Smith, S.O. (1994) *J. Magn. Reson. Ser. A*, **110**, 219–227.

Mobley, P.W., Lee, H.F., Curtain, C.C., Kirkpatrick, A., Waring, A.J. and Gordon, L.M. (1995) *Biochim. Biophys. Acta*, **1271**, 304–314.

Murphy, 3rd, O.J., Kovacs, F.A., Sicard, E.L. and Thompson, L.K. (2001) *Biochemistry*, **40**, 1358–1366.

Nieva, J.L., Nir, S., Muga, A., Goni, F.M. and Wilschut, J. (1994) *Biochemistry*, **33**, 3201–3209.

Oas, T.G., Hartzell, C.J., McMahon, T.J., Drobny, G.P. and Dahlquist, F.W. (1987) *J. Am. Chem. Soc.*, **109**, 5956–5962.

Pereira, F.B., Goni, F.M., Muga, A. and Nieva, J.L. (1997) *Biophys. J.*, **73**, 1977–1986.

Pereira, F.B., Goni, F.M. and Nieva, J.L. (1995) *FEBS Lett.*, **362**, 243–246.

Perry, A., Stypa, M.P., Foster, J.A. and Kumashiro, K.K. (2002) *J. Am. Chem. Soc.*, **124**, 6832–6833.

Press, W.H., Teukolsky, S.A., Vetterling, W.T. and Flannery, B.P. (1996) *Numerical Recipes in FORTRAN 77: The Art of Scientific Computing*, Cambridge, New York.

Rafalski, M., Lear, J.D. and DeGrado, W.F. (1990) *Biochemistry*, **29**, 7917–7922.

Saez-Cirion, A. and Nieva, J.L. (2002) *Biochim. Biophys. Acta-Biomembr.*, **1564**, 57–65.

Schaal, H., Klein, M., Gehrmann, P., Adams, O. and Scheid, A. (1995) *J. Virol.*, **69**, 3308–3314.

Smith, R., Separovic, F., Milne, T.J., Whittaker, A., Bennett, F.M., Cornell, B.A. and Makriyannis, A. (1994) *J. Mol. Biol.*, **241**, 456–466.

Spera, S. and Bax, A. (1991) *J. Am. Chem. Soc.*, **113**, 5490–5492.

States, D.J., Haberkorn, R.A. and Ruben, D.J. (1982) *J. Magn. Reson.*, **48**, 286–292.

Subramanian, E. and Lalitha, V. (1983) *Biopolymers*, **22**, 833–838.

Tomita, Y., O'Connor, E.J. and McDermott, A. (1994) *J. Am. Chem. Soc.*, **116**, 8766–8771.

Tycko, R. and Berger, A.E. (1999) *J. Magn. Reson.*, **141**, 141–147.

Tycko, R. and Dabbagh, G. (1991) *J. Am. Chem. Soc.*, **113**, 3592–3593.

Tycko, R., Weliky, D.P. and Berger, A.E. (1996) *J. Chem. Phys.*, **105**, 7915–7930.

Weliky, D.P. and Tycko, R. (1996) *J. Am. Chem. Soc.*, **118**, 8487–8488.

Weliky, D.P., Bennett, A.E., Zvi, A., Anglister, J., Steinbach, P.J. and Tycko, R. (1999) *Nat. Struct. Biol.*, **6**, 141–145.

Wishart, D.S., Sykes, B.D. and Richards, F.M. (1991) *J. Mol. Biol.*, **222**, 311–333.

Yang, J., Gabrys, C.M. and Weliky, D.P. (2001a) *Biochemistry*, **40**, 8126–8137.

Yang, J., Parkanzky, P.D., Khunte, B.A., Canlas, C.G., Yang, R., Gabrys, C.M. and Weliky, D.P. (2001b) *J. Mol. Graph. Model.*, **19**, 129–135.